ACS OMEGA

http://pubs.acs.org/journal/acsodf

Article

Development of a Novel Dual-Order Protein-Based Nanodelivery Carrier That Rapidly Targets Low-Grade Gliomas with Microscopic Metastasis *in Vivo*

Zihao Wang, Xinbo Zhou, Yuru Xu, Shiyong Fan, Ning Tian, Wenyuan Zhang, Fugeng Sheng,* Jian Lin,* and Wu Zhong*

Cite This: *ACS Omega* 2020, 5, 20653−20663

Read Online

ACCESS | Metrics & More | Article Recommendations | Supporting Information

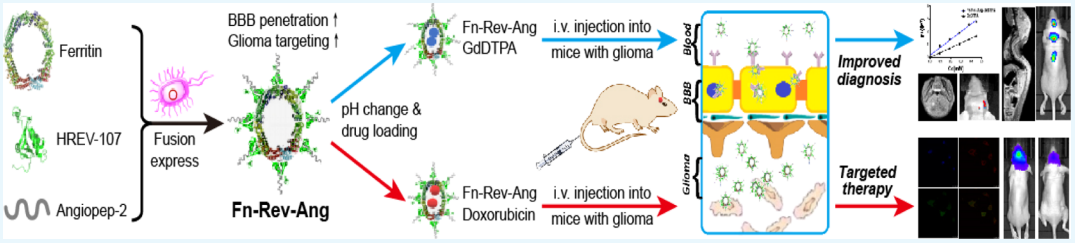

ABSTRACT: Clinically diagnosing low-grade gliomas and microscopic metastatic tumors in the spinal cord using magnetic resonance imaging (MRI) is challenging, as the blood−brain barrier (BBB) almost completely excludes the MRI contrast agent gadopentetate dimeglumine, GdDTPA (Magnevist), from the brain. The development of a more efficient, safe, and broad-spectrum glioma diagnosis and treatment would therefore have a great clinical value. Based on the high expression levels of both transferrin receptor 1 (TfR1) and low-density lipoprotein receptor-related protein 1 (LRP1) in BBB-related cells and glioma cells, we designed a novel protein nanoparticle, ferritin-HREV107-Angiopep-2 (Fn-Rev-Ang). We found that Fn-Rev-Ang rapidly crossed the BBB in mice and had drug-loading properties. Moreover, the brain MRI signal intensity ratio associated with Fn-Rev-Ang-GdDTPA was higher than that associated with Fn-GdDTPA alone. Importantly, gliomas with diameters below 1 mm and microscopic metastatic tumors in the spinal cord were successfully detected in mice by MRI with Fn-Rev-Ang-GdDTPA, which is not possible using the current clinical MRI technology. In addition, Fn-Rev-Ang-loaded doxorubicin had a strong inhibitory effect on mouse brain gliomas and their metastasis, which significantly prolonged the animal survival time. Thus, our newly constructed Fn-Rev-Ang nanodelivery carrier may help expand the use of MRI to the early diagnosis and treatment of microscopic tumors, thereby offering a possible basis for improving the survival rate of patients with gliomas and microscopic spinal metastatic tumors.

INTRODUCTION

Brain tumors, especially gliomas, are the most common malignant tumors in both children and adults.[1] Some types of gliomas, such as glioblastoma (GBM), are characterized by metastatic growth and unclear tumor boundaries, which in turn make them difficult to treat with surgery.[2] The average survival of GBM patients is approximately 5−12 months with aggressive surgical resection and conventional therapy.[3]

T1-weighted magnetic resonance imaging (MRI), with or without gadolinium (Gd), is the major imaging modality for diagnosis and therapeutic evaluation.[4] However, significant MRI signal enhancement cannot be detected in low-grade gliomas or microscopic brain tumors because clinical contrast agents such as GdDTPA (Magnevist) cannot cross the blood−brain barrier (BBB).[5]

Aside from contrast agents, the BBB similarly hinders chemotherapeutic drugs from entering brain tissues and reaching glioma tumors. In addition, there have been no reports of the diagnosis of micrometastatic tumors in the slender spinal cords of mice by MRI. Therefore, there is an urgent need to develop a diagnostic reagent and chemotherapeutic drug carrier that is capable of rapidly crossing the BBB with high glioma-targeting efficiency.

The existing technologies that are being used are limited by a long target imaging time, low drug delivery efficiency to the brain and tumor, and nanomaterial toxicity. A two-order nanoprobe was developed by Li's group for T1-weighted MRI of brain tumors.[6] Cyclic [RGDyK] peptides, targeted with high affinity by tumor angiogenesis, and BBB-permeable angiopep-2 peptides[7] have been conjugated with the PAMAM G5 dendrimer which is a poly(amidoamine) dendrimer-based

Received: June 25, 2020
Accepted: July 27, 2020
Published: August 7, 2020

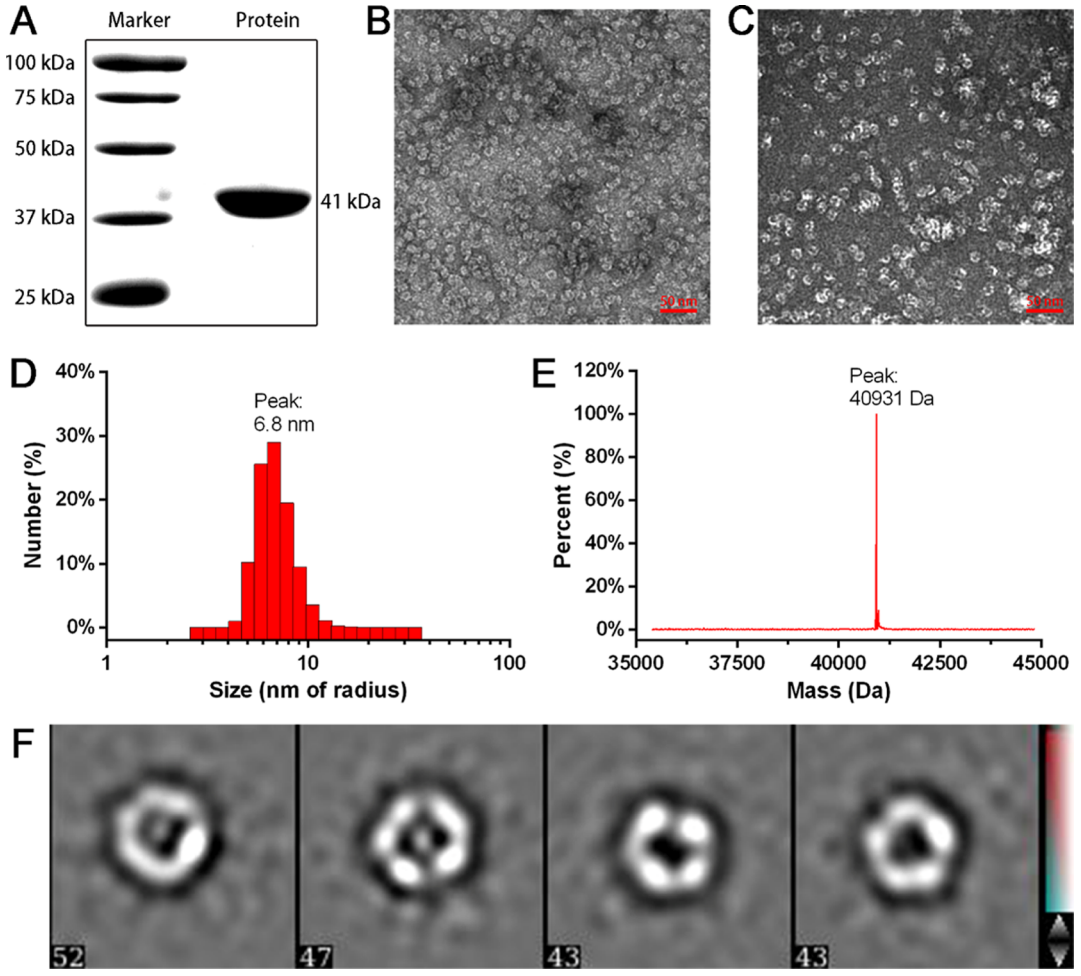

Figure 1. Preparation and characterization of Fn-Rev-Ang nanoparticles. (A) SDS-PAGE band showing the size of the Fn-Rev-Ang protein. (B) TEM image of Fn-Rev-Ang, scale bar = 50 nm. (C) TEM image of reassociated Fn-Rev-Ang, scale bar = 50 nm. (D) DLS analysis of Fn-Rev-Ang showing the size range of Fn-Rev-Ang at pH 7.4. (E) ESI-MS analysis of the molecular weight of Fn-Rev-Ang. (F) Focus of one Fn-Rev-Ang nanoparticle with imaging at different angles.

multifunctional cancer therapeutic conjugate to increase glioma targeting. Dendrimers result in unavoidable cytotoxicity.[8] Furthermore, despite the ability of some existing imaging and drug-delivery techniques to cross the BBB, the failure of these techniques to allow the imaging of tumors that are less than 1 mm in diameter or of tumors that have spread to the spinal cord restrict their clinical use.

Protein nanoparticles have the unique advantage of low toxicity in glioma-targeted imaging and treatment, as they can be degraded *in vivo*.[9,10] Of particular interest is ferritin, a natural nanoparticle that regulates iron storage and has the potential to act as a highly effective and biodegradable carrier for imaging and therapy.[11−15] Ferritin consists of 24 subunits organized in a spherical structure, with outer and inner cavity diameters of 12 nm and 8 nm, respectively.[16] In addition, ferritin dissociates at pH 2.0 and reassociates at pH 7.4.[17] Because of these self-assembled characteristics, previous studies have demonstrated that compounds such as Gd-$HPDO_3A$,[18] cisplatin,[19] and ^{235}U[20] can be loaded into the empty inner cavity of ferritin for imaging or therapy. In addition, it has been reported that ferritin can cross the BBB through the action of TfR1, which is overexpressed not only in a variety of tumor cell types[20,21] but also in the BBB.[22] Indeed, the synthesized ferritin nanoparticles with a magnetite core, a notable MR contrast enhancement of brain gliomas orthotopically xenografted into mice, were visible on T2-weighted MR images.[22] However, it would take at least 2 h after injection of the M−ferritin nanoparticles to obtain MR images of glioma. In addition, the need for T2-weighted MR imaging also restricts further application of magnetite core ferritin nanoparticles in the clinic.

Gliomas are known to be genetically heterogeneous and complex. For example, the dysregulation of TfR expression in glioma cells is often only 3−5-fold higher than that in normal cells.[23] Indeed, insufficient expression of glioma tissue receptors generally impairs the efficacy of single-target glioma drug delivery. To enhance their diagnostic and treatment effects, the development of a targeted glioma drug delivery system based on a traditional ferritin nanotechnology with improved safety, efficacy, and broad-spectrum glioma delivery capability is urgently needed.

In this work, we developed a novel dual-order targeted imaging and therapy strategy based on lipoprotein receptor-related protein 1 (LRP1)[23] and transferrin receptor 1 (TfR1),[24] which are expressed on the surface of both brain capillary endothelial cells in the BBB[25] and in various types of gliomas. LRP1 is a single-pass transmembrane receptor that is highly expressed in brain endothelial cells. Fusion of the LRP1

https://dx.doi.org/10.1021/acsomega.0c03073
ACS Omega 2020, 5, 20653−20663

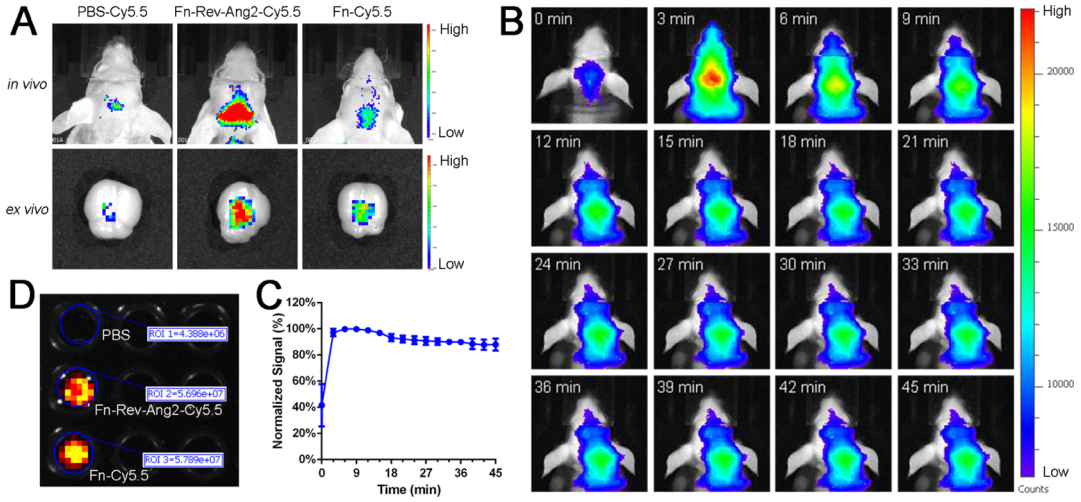

Figure 2. Fn-Rev-Ang-Cy5.5 crossed the BBB *in vivo*. (A) Fluorescence imaging of Cy5.5-PBS (left), Fn-Rev-Ang-Cy5.5 (middle), and Fn-Cy5.5 (right) *in vivo* and *ex vivo* following the injection of each solution into the tail vein. (B,C) Fluorescence imaging *in vivo*. Mice were injected i.v. with Fn-Rev-Ang-Cy5.5 and were imaged every 3 min for 45 min (D) Fluorescence imaging showing that the number of Fn and the number of Fn-Rev-Ang-labeled fluorescence were the same.

protein ligand peptide angiopep-2 to a ferritin nanoparticle ferritin-HREV107-Angiopep-2 (Fn-Rev-Ang) achieved dual targeting for both the BBB and gliomas. Angiopep-2 is a short peptide consisting of 19 amino acids with the amino acid sequence TFFYGGSRGKRNNFKTEEY and a molecular weight of 2.4 kDa, which is a ligand for low-density lipoprotein receptor-related protein (LRP). We found that Fn-Rev-Ang nanoparticles had rapid BBB permeability and drug-loading properties. Fn-Rev-Ang-GdDTPA showed a significant increase in the MR signal intensity ratio value in the brains of mice (up to 30%) compared to only a 3% increase with Fn-GdDTPA. Importantly, gliomas with a diameter below 1 mm and microscopic metastatic tumors in the spinal cord were successfully detected by T1-weighted MRI using Fn-Rev-Ang-loaded GdDTPA, which is currently the limit of clinical MRI technology. In addition, Fn-Rev-Ang-loaded doxorubicin (Dox) had a marked inhibitory effect on brain gliomas and their metastasis in mice. Our results indicate that Fn-Rev-Ang nanoparticles can broaden the application of Magnevist in the clinical diagnosis of microscopic tumors in both the brain and spinal cord.

RESULTS

Design, Synthesis, and Characterization of Fn-Rev-Ang. We initially attempted to synthesize a dual-targeted novel nanoparticle by direct expression of the peptide angiopep-2 fused to the N-terminus of ferritin. The peptide angiopep-2 was fused to the N-terminus of ferritin and then expressed in *Escherichia coli*. Unfortunately, Fn-Ang was expressed mostly as inclusion bodies in *E. coli*. Proteins could not fold exactly and exist in inclusion bodies. Meanwhile, the expression of the peptide RGD4C fused to the N-terminus of ferritin resulted in a low yield and poor solubility.[26,27]

In order to express a soluble dual-order targeted nanoparticle, we next used HREV-107 as a peptide-displaying protein. HREV-107 inhibits tumor cell growth and induces apoptosis,[28] and it has 3 α-helices, 6 β-sheets, and a large loop domain (P38-K57), which is suitable for displaying peptides. The P38-K57 domain does not participate in the generation of hydrophobic structures. As such, modified peptides targeted to the P38-K57 domain of HREV-107 can maintain the physiological functions of the peptide.

With the favorable characteristics of HREV-107 in mind, we next integrated angiopep-2, HREV-107, ferritin, and histidine tags to express a dual-targeted protein nanoparticle, Fn-Rev-Ang. Histidine tags are for convenience of protein purification. The Fn-Rev-Ang fusion protein was successfully purified with NTA-Ni affinity chromatography in a high yield (75 mg per liter in *E. coli*). Sodium dodecyl sulfate (SDS) gel chromatography of the purified Fn-Rev-Ang revealed only one band with a molecular weight close to 41 kDa (Figure 1A), and electrospray ionization mass spectrometry (ESI-MS) yielded a similar molecular weight of 40.93 kDa (Figure 1E). The purified Fn-Rev-Ang nanoparticles were next analyzed by transmission electron microscopy (TEM). Both Fn-Rev-Ang and reassembled Fn-Rev-Ang showed spherical morphologies (Figure 1B,C,F). Additionally, TEM showed that Fn-Rev-Ang had a narrow distribution at approximately 6.8 nm (Figure 1D) at pH 7.4. To investigate the diameter of Fn-Rev-Ang at different pH values, we adjusted the pH of the nanoparticle solution diminishingly from 7.4 to 2.0, and the Fn-Rev-Ang nanoparticle diameter increased from 6.8 to 1000 nm with a decrease in pH from 7.4 to 5.5 (Figure S1). However, there was no similar increase in diameter with decreasing pH observed for the Fn nanoparticles (Figure S2). As tumors have an acidic microenvironment, this result suggests that Fn-Rev-Ang nanoparticles could increase in size in the tumor microenvironment.

Fn-Rev-Ang Crosses the BBB More Efficiently Than Fn. To compare the abilities of Fn-Rev-Ang and Fn to penetrate the BBB, Fn-Rev-Ang and Fn were labeled with the fluorescent dye Cy5.5 and intravenously injected into mice. First, a desalting column was used to remove the free Cy5.5 to obtain purified Fn-Cy5.5 and Fn-Rev-Ang-Cy5.5. The fluorescence intensities were normalized among the Fn-Rev-Ang-Cy5.5, Fn-Cy5.5, and Cy5.5 (negative control) samples (Figure 2D). Then, BALB/c nude mice with body weights of approximately 20 g were injected (*via* tail vein) with 100 μL of either Fn-Rev-Ang-Cy5.5 (2.3 mg/mL), Fn-Cy5.5 (2.7 mg/mL), or Cy5.5 solution (n = 5). *In vivo* brain imaging after

https://dx.doi.org/10.1021/acsomega.0c03073
ACS Omega 2020, 5, 20653−20663

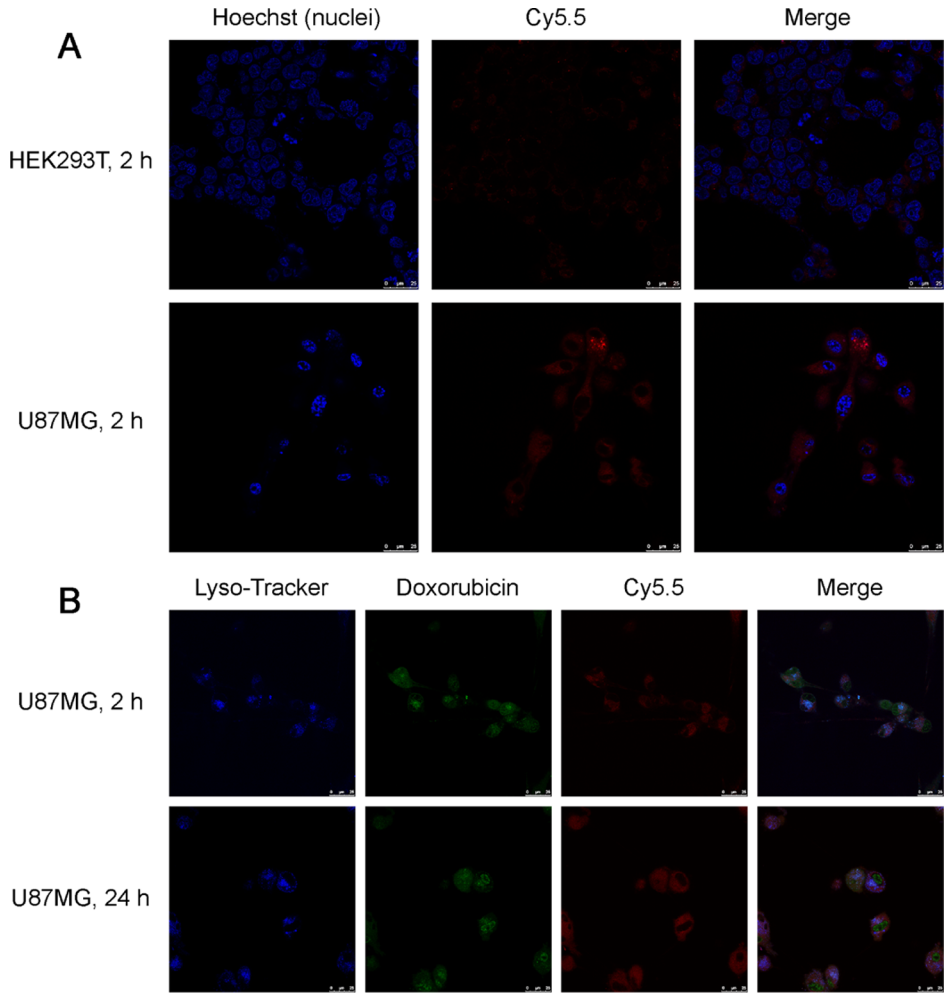

Figure 3. (A) Confocal imaging of the intracellular uptake of Fn-Rev-Ang-Dox-Cy5.5 in HEK293T cells at 2 h of incubation (top row) and in U87MG cells at 2 h. Scale bar, 25 μm; Hoechst, blue; Cy5.5, red. (B) Confocal imaging of the intracellular uptake of Fn-Rev-Ang-Dox-Cy5.5 in U87MG cells at 2 and 24 h. Scale bar, 25 μm; LysoTracker, blue; Dox, green; Cy5.5, red.

injection revealed that Fn-Rev-Ang-Cy5.5 had the most intense fluorescent signal in the brain, followed by Fn-Cy5.5 and Cy5.5 (Figure 2A,B). After transcardial perfusion, the brain imaging (Figure 2A, *ex vivo*) showed similar results to live imaging. The purpose of transcardial perfusion is to prevent fluorescent molecules from remaining in the blood vessels. The results indicated that Fn-Rev-Ang crosses the BBB more efficiently than Fn (Figures 2B,C and S3). Biodistribution for Fn-Rev-Ang-Cy5.5 in nude mice is presented, showing all collected organs (Figure S4).

Fn-Rev-Ang Nanoparticles Showed a Greater Accumulation in Brain Glioma Cells Than in Noncancerous Kidney Cells. As both the Fn receptor TfR1 and the Ang receptor LRP1 are overexpressed on various glioma cell types, we investigated whether Fn-Rev-Ang shows a greater accumulation in, and thus specific targeting to, U87MG cells (a brain glioma cell line) than in HEK293T cells (a kidney epithelial cell line). Fn-Rev-Ang was first loaded with Dox and then labeled with Cy5.5 (Fn-Rev-Ang-Dox-Cy5.5). Then, U87MG and HEK293T cells were incubated with Fn-Rev-Ang-Dox-Cy5.5 (2 mg/mL) separately for different lengths of time before observation by fluorescence microscopy. Fn-Rev-Ang-Dox-Cy5.5 accumulated rapidly in the cytoplasm of U87MG cells within 40 min of incubation at 37 °C (Figures S5). After 2 h of incubation, both Cy5.5 and Dox fluorescence in U87MG cells were much higher than the respective signals in HEK293T cells (Figures 3A, S6, and S7). Dox and Cy5.5 fluorescence were observed in the cytoplasm of U87MG cells after 2 h of incubation. After 24 h of incubation, the Dox signal was intensely expressed in the nuclei, while the Cy5.5 signal remained in the cytoplasm of the U87MG cells, indicating the release of Dox from the nanoparticle (Figure 3B). These results indicated that Fn-Rev-Ang rapidly attained a higher level of accumulation in cancer cells than in noncancerous kidney cells.

Loading of Fn-Rev-Ang with GdDTPA (Magnevist) Improved MRI of Microscopic Tumors in the Brain and Spinal Cord. In clinical treatment, glioma has a characteristic of metastasis. The brain is connected to the spinal cord by the cerebrospinal fluid. Usually, gliomas travel along the cerebrospinal fluid from the brain to the cervical, thoracic, and lumbar vertebrae. Many patients become paralyzed because of the pressure and edema of the glioma in the thoracic and lumbar vertebrae. The mouse model established by us also confirmed this view. Using fluorescence imaging and CT imaging techniques, we found that the tumor-bearing mice in the brain were slow to move, and the limbs were inconvenient to move. It was found that there were obvious tumor signals in the spinal cord of mice. The coronal, sagittal, axial, and 3D reconstruction images of mice are shown in

https://dx.doi.org/10.1021/acsomega.0c03073
ACS Omega 2020, 5, 20653−20663

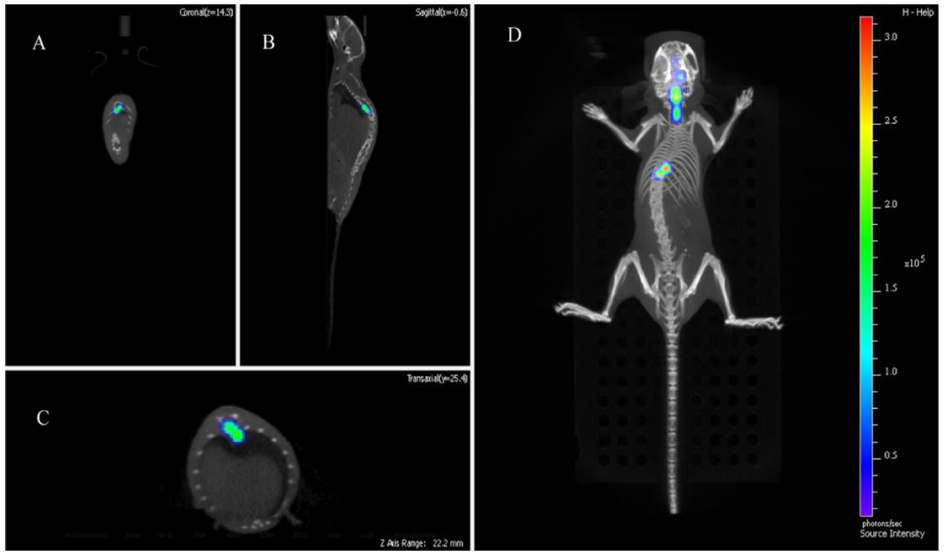

Figure 4. Fluorescence imaging and CT imaging were used to observe the metastatic pathway of brain tumors in mice. (A) The coronal view shows the green part of the spinal cord as tumor cells. (B) Sagittal view, the green part is the tumor cells. (C) The axial view shows the tumor cells in green. (D) 3D imaging of mice showed that after injection of tumor cells into the right side of the brain, the tumor cells metastasize from the spinal cord to the thoracic vertebra.

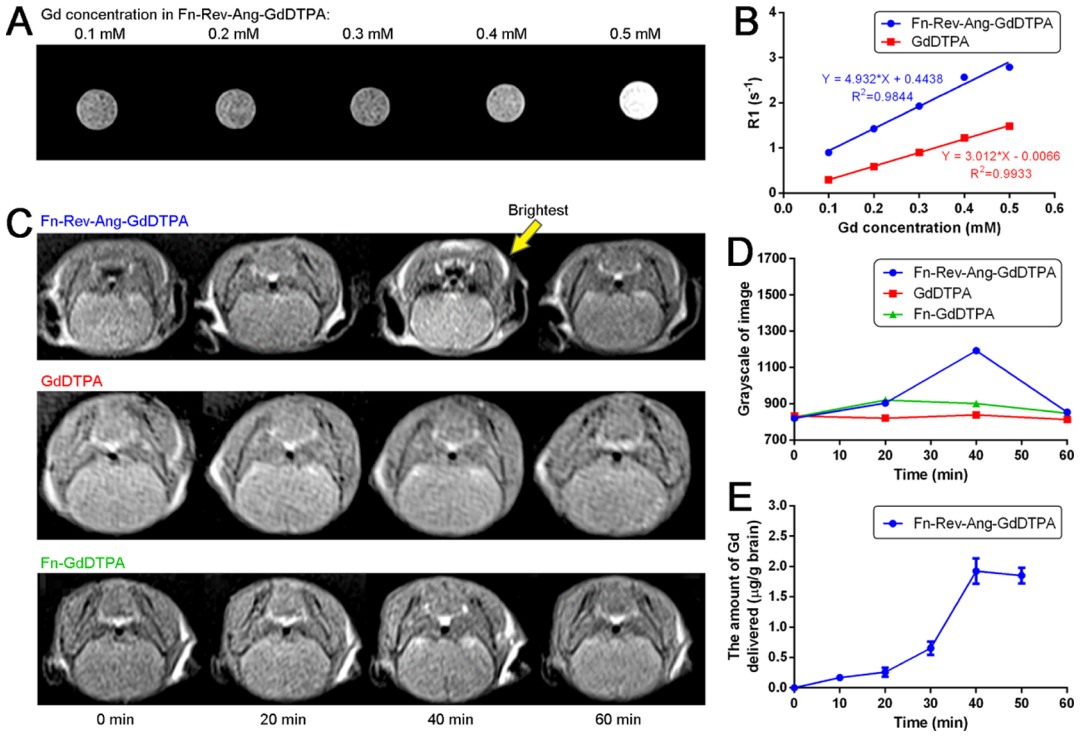

Figure 5. (A) T1 MR imaging in a 2 mL centrifuge tube of Fn-Rev-Ang-GdDTPA containing various concentrations of Gd. (B) Relaxation time of Fn-Rev-Ang-GdDTPA *vs* free GdDTPA. Linear regression was used with R^2 reported. (C) *In vivo* T1 MRI of Fn-Rev-Ang-GdDTPA, GdDTPA, and Fn-GdDTPA following i.v. administration in healthy mice. (D) Brain T1 MRI signal intensity changes over time after i.v. administration of Fn-Rev-Ang-GdDTPA, GdDTPA, and Fn-GdDTPA. The *y* axis represents the grayscale of image. (E) Time-course of the expression of Gd in mouse brains following i.v. injection of Fn-Rev-Ang-GdDTPA, as assessed by ICP−MS.

Figure 4A−D. In addition to tumor signals in the brain of mice injected *in situ*, tumor cells can be transferred to cervical, thoracic, and caudal vertebrae.

The mouse model established by us also confirmed this view. Using fluorescence imaging and CT imaging techniques, we found that the tumor-bearing mice in the brain were slow to move, and the limbs were inconvenient to move. It was found that there were obvious tumor signals in the spinal cord of mice. The coronal, sagittal, axial, and 3D reconstruction images of mice are shown in Figure 4A−D. In addition to tumor signals in the brain of mice injected *in situ*, tumor cells can be transferred to cervical, thoracic, and caudal vertebrae.

In order to investigate whether the Fn-Rev-Ang nanoparticle can be harnessed for the MRI of gliomas, we next loaded an

https://dx.doi.org/10.1021/acsomega.0c03073
ACS Omega 2020, 5, 20653−20663

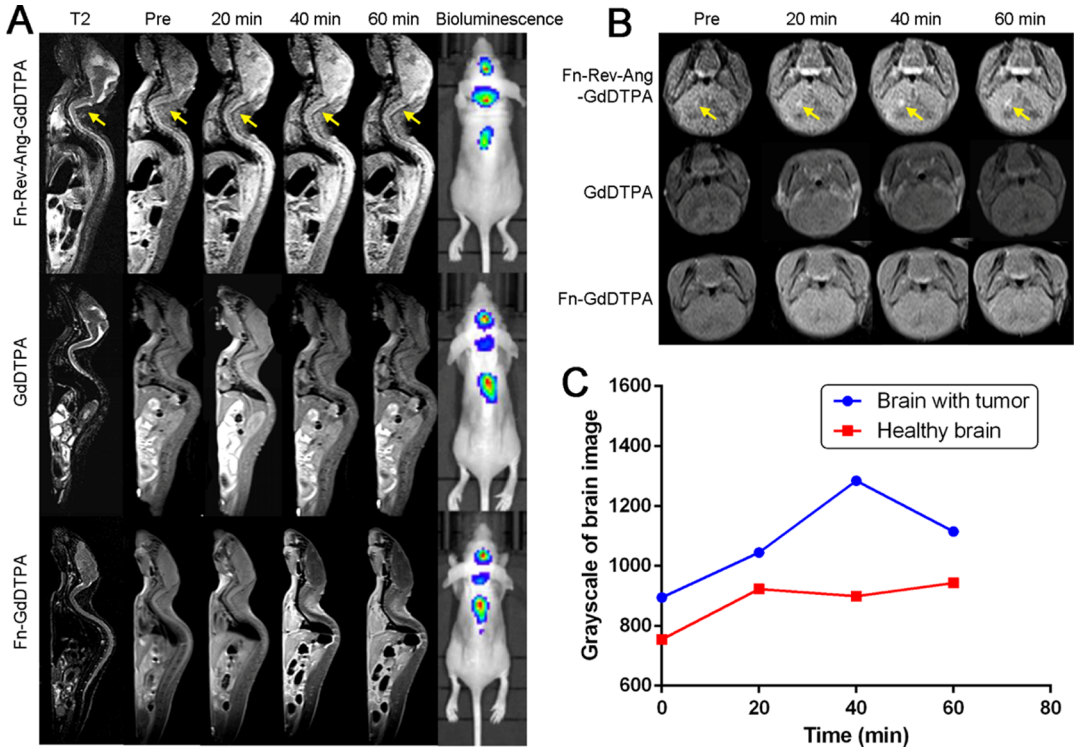

Figure 6. (A) *In vivo* T2 MR imaging and bioluminescence imaging for spinal cord metastatic glioma tumors induced by the injection of U87MG cells into the right caudate of mice. Imaging was conducted before and at 20, 40, and 60 min post-injection of Fn-Rev-Ang-GdDTPA (top row), GdDTPA (middle row), and Fn-GdDTPA. (B) *In vivo* T1 MR images of glioma-bearing mice subjected to the same experiment as in (B). Highly positive Gd signals in tumors following the injection of Fn-Rev-Ang-GdDTPA are shown by the arrows. (C) Signal intensity change in tumor tissues over time. The *y* axis represents the grayscale of image.

MRI contrast agent GdDTPA (Magnevist) into the Fn-Rev-Ang nanoparticle. The concentration of loaded Gd was first assessed by inductively coupled plasma mass spectrometry (ICP−MS) and NanoDrop. Using ICP−MS quantification, Gd was found to be 36.18 mg/L, with a molarity of 2.3×10^{-4} M. As the protein concentration of Fn-Rev-Ang-GdDTPA was found to be 1.01×10^{-6} M, we conclude that on average, each Fn-Rev-Ang nanoparticle cages 227 GdDTPA molecules. In addition, the relaxation rate of Fn-Rev-Ang-GdDTPA was 4.93 mM^{-1} s^{-1} (Figure 5A,B), while the free GdDTPA relaxation rate was 3.01 mM^{-1} s^{-1}.[29]

We next investigated the ability of Fn-Rev-Ang-GdDTPA, Fn-GdDTPA, and GdDTPA to penetrate the BBB in mice. Fn-Rev-Ang-GdDTPA, Fn-GdDTPA, and GdDTPA were prepared as solutions with a Gd concentration of 0.01 mmol/kg, and these solutions were then injected through the tail veins of mice. MRI T1 scanning was performed, and the time of restoration (TR) was set to 500 ms, the time of echo (TE) was set to 11 ms, the flip angle was set at 150°, and the thickness was set to 0.8 mm. The scan was performed every 90 s for 2 h following injection. GdDTPA-injected mice did not show an obvious increase in brain the MR signal intensity ratio value, although increases in the MR signal intensity ratio were observed in the kidneys and bladder. Mice injected with Fn-GdDTPA showed only a 3% increase in the brain MR signal intensity ratio, and also increases in the kidneys, bladder, and especially the gallbladder. This result shows that most of the ferritin-carried GdDTPA is metabolized through the biliary tract, as opposed to being excreted from the kidneys. By contrast, mice injected with Fn-Rev-Ang-GdDTPA showed an increase in the brain MR signal intensity ratio of up to 30% (Image gray value) at 40 min postinjection (Figure 5C). Sixty minutes after the injection, the brain MR signal intensity ratio value decreased to levels similar to those before injection. Similar to injection with Fn-GdDTPA, the mice injected with Fn-Rev-Ang-GdDTPA did not display changes in the MR signal intensity ratio values in the bladder and kidneys, but the livers and gallbladders did show increases in the MR imaging signal intensity ratio (Figure 5D), which suggests that Fn-Rev-Ang-GdDTPA is also excreted through the biliary tract. Taken together, these three sets of experiments show that GdDTPA carried by Fn-Rev-Ang can readily cross the BBB and, in turn, intensify the MRI signal. In clinical trials, GdDTPA has caused nephrogenic systemic fibrosis.[30] The FDA warns physicians to exercise caution when using a gadolinium-based contrast agent in patients with renal disease. However, if carried by Fn-Rev-Ang, the metabolic pathway of Gd can be altered such that Gd would not enter the kidneys, thereby reducing its toxicity to the kidney cells. Similarly, the literature has reported that Gd-lipid nanoparticles[31] were also eliminated predominately through the biliary system instead of through the renal system.

To further quantify the Gd content in mouse brains after the tail vein injection of Fn-Rev-Ang-GdDTPA, and thus the ability of Fn-Rev-Ang-GdDTPA to cross the BBB, we used ICP−MS for pharmacokinetic and tissue expression studies. Three mice from Fn-Rev-Ang-GdDTPA, Fn-GdDTPA, and GdDTPA groups were sacrificed every 20 min after injection. After transcardial perfusion, the brains were removed and digested. We found that the greatest yield of brain-derived Gd (1.8 μg/g) was observed 40 min after the injection of Fn-Rev-Ang-GdDTPA, and decreased gradually thereafter. This change in the Gd content was consistent with the timing of the change

https://dx.doi.org/10.1021/acsomega.0c03073
ACS Omega 2020, 5, 20653−20663

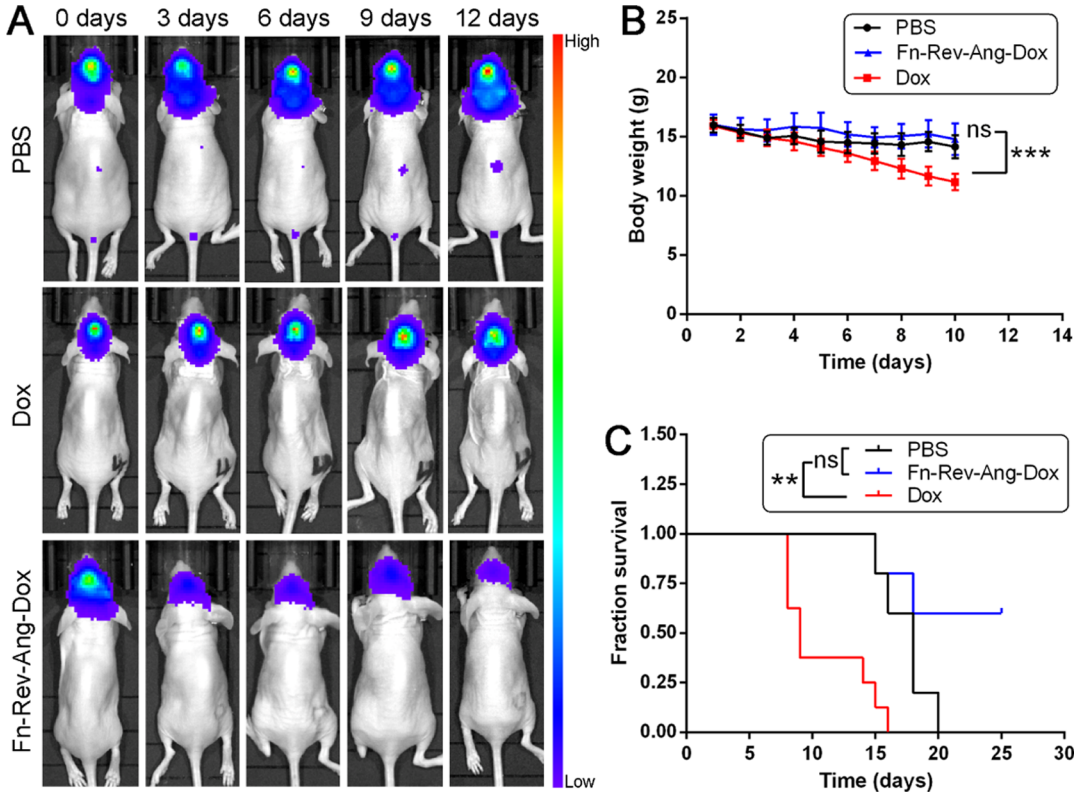

Figure 7. (A) Bioluminescence imaging showing the antitumor effect over time of Fn-Rev-Ang-Dox (bottom row) compared to PBS and Dox injected iv or intracerebroventricular into glioma-bearing mice. (B) Body weight change in the PBS, Fn-Rev-Ang-Dox, and Dox groups. Data are presented as mean ± SD (n = 5−8). One-way ANOVA and Tukey's multiple comparison test were performed on groups of day 10. (C) Average change in the body weight after treatment. The log-rank (Mantel−Cox) test was used for comparisons of survival curves. ns: not significant (p > 0.05). **p < 0.01. ***p < 0.001.

in the MRI signal intensity. These results indicated that Fn-Rev-Ang enabled the concentration of GdDTPA (Magnevist) to increase in the brain relative to Fn-GdDTPA or free GdDTPA.

We next investigated whether Fn-Rev-Ang-GdDTPA could be used for the detection of microscopic gliomas in mice. Using T1/2 MRI, we first demonstrated that the MRI signal was enhanced at tumor sites *in vivo* following the tail vein injection of Fn-Rev-Ang-GdDTPA into mice with U87MG tumor xenografts (Figure 6A,B). Importantly, the MRI signal was enhanced not only at the site of injection but also at the site of metastasis in the spinal cord. The MRI signal enhancement in the right brain hemisphere was observed as soon as 40 min postinjection (Figure 6C). Moreover, the MR signal intensity ratio between the tumor (the brain and the spinal cord) and normal (muscle) noncancerous tissues continued to increase after injection of Fn-Rev-Ang-GdDTPA, and the maximum value of the ratio (1.3) was reached after 40 min.

Next, glioma-bearing mice were tail vein injected with Fn-Rev-Ang-GdDTPA, transcardially perfused 40 min later, and the left and right sides of the brain were separated. After digestion, the Gd content was determined in each side of the brain using ICP−MS. The results show that the brain Gd content was 14% higher in the right hemisphere (tumor tissues) than in the left hemisphere (normal tissues). The higher concentration of Fn-Rev-Ang-Gd in the right hemisphere (tumor site) suggested that Fn-Rev-Ang-Gd nanoparticles had a certain degree of enrichment in brain gliomas (Figure S8). MRI scans of organ distribution, including the bladder, brain, tumor, and muscle are shown as Figure S9.

To confirm that the microscopic tumors had not yet compromised the BBB, TEM was used to assess the integrity of the BBB. The brain vasculature of the mice injected with Fn-Rev-Ang-Gd remained intact, with a complete basement membrane and tight junctions. Therefore, the Fn-Rev-Ang-Gd-mediated MRI signal enhancement of the microscopic tumors in the brain was not due to damage to the BBB.

In addition, to explore the toxicity of Fn-Rev-Ang-GdDTPA, healthy mice that were tail vein injected with Fn-Rev-Ang-GdDTPA were sacrificed 1, 7, and 14 days postinjection. After transcardial perfusion, the hearts, livers, spleens, lungs, and kidneys were stained with hematoxylin and eosin (H&E stain) (Figure S10). Pathological analysis showed that the injection of Fn-Rev-Ang-GdDTPA did not cause tissue abnormalities. The organs show normal size and cellular morphology.

Taken together, these experiments show that Fn-Rev-Ang nanoparticles loaded with GdDTPA can facilitate MRI-enhanced imaging of microscopic tumors (1 mm × 1 mm) in brains with an intact BBB. In addition, glioma metastases in the spinal cord were successfully observed following the injection of Fn-Rev-Ang-GdDTPA. These results show that Fn-Rev-Ang-GdDTPA has the ability to not only cross the BBB but also target glioma tumor cells in both the brain and spinal cord.

To verify the permeability of BBB in tumor-bearing mice, we attempted TEM observation after imaging (MRI, bioluminescence imaging, and H&E staining sections). It was found that the basal membrane of the BBB was intact and the tight

https://dx.doi.org/10.1021/acsomega.0c03073
ACS Omega 2020, 5, 20653−20663

junction was still present. These results suggest that it is not damage to the BBB that causes drug delivery to the brain (Figure S11).

Fn-Rev-Ang-Dox Therapy Experiment. Dox, an anthraquinone antibiotic,[32] is widely used in cancer therapy. However, Dox has limited applications in the treatment of brain tumors because it cannot efficiently cross the BBB. Therefore, we investigated whether Fn-Rev-Ang might improve the therapeutic effect of Dox in brain tumors relative to free Dox or phosphate-buffered saline (PBS, control).

A glioma-bearing model was established that was same as the previous model. Ten days after luciferase-expressing glioma cell xenografts *in vivo*, mice were grouped (n = 5−8) and tail vein injected with PBS, free Dox (10 mg/kg), or Fn-Rev-Ang-Dox (10 mg/kg) every 2 days for 15 days. The efficacy of Dox in treating the luciferase-expressing gliomas was determined by measuring the tumor bioluminescence intensity. Twenty minutes after luciferin injection (450 mg/kg), the mice were imaged, and the regions of interest (ROIs) were selected to measure the intensity of the bioluminescence. Living Image software, Lumina XRMS Series III *in vivo* imaging system (IVIS) (PerkinElmer Inc.), can calculate the ROI of luciferase activity, which is expressed as photons/s/cm^2/sr. Mice from the Fn-Rev-Ang-Dox-treated group showed weaker bioluminescence intensities than those from the free Dox or PBS groups. As shown in Figure 7, gliomas from the PBS-treated group had metastasized to the spinal cord, and the development of these metastasized tumors was clearly visible from the tumor bioluminescence intensity. An increase in tumor bioluminescence intensity was observed. In the Dox treatment group, there was no significant effect of treatment on bioluminescence (Figure 7A). The average survival times for the mice treated with Fn-Rev-Ang-Dox, free Dox, and PBS were 23.6, 17.4, and 10.9 days, respectively (Figure 7B). This result indicates that the antiglioma effect of Fn-Rev-Ang-Dox was due to the specific crossing of the BBB and delivery of the drug to the glioma targeting both LRP1 and TfR1. We noted a decrease in body weight in PBS, free Dox, and Fn-Rev-Ang-Dox groups of mice (Figure 7C), which might be caused by the constriction of nerves caused by the glioma cells leading to a decrease in food intake. The log-rank (Mantel−Cox) test was used for the comparison of survival curves. ns: not significant ($p > 0.05$). **$p < 0.01$. ***$p < 0.001$. The significant loss in body weight in the free Dox treatment group was attributed to the toxicity of Dox (Figure 7).

DISCUSSION

Although several research groups have reported that ferritin-based nanoparticles can be applied for the imaging and treatment of glioma in the brain, our results showed that only a small amount of ferritin nanoparticles could efficiently reach the brain because of the BBB, which would greatly limit their application in the clinic.

To improve the ability of the ferritin nanoparticles to cross the BBB, here we fused ferritin with the protein HREV107 and the peptide angiopep-2 (Fn-Rev-Ang). The long loop region of HREV107 is suitable for displaying the angiopep-2 peptide on the surface of the nanoparticle. Compared with ferritin alone, Fn-Rev-Ang nanoparticles more rapidly crossed the BBB and showed greater accumulation in the brain. In addition, the expression of Fn-Rev-Ang was high (75 mg/L of Lysogeny broth medium) in *E. coli*, which implied that a large quantity of nanoparticles can be easily synthesized in the future.

Although GdDTPA is widely used for the diagnosis of brain tumors, the limitation of its use is that the BBB must be disrupted. Only large tumors which have disrupted the BBB can successfully be detected. As low-grade gliomas do not compromise the BBB, and GdDTPA cannot cross the BBB, their diagnosis remains a challenge as they cannot be detected by MRI. Similarly, it is impossible to diagnose microscopic metastatic tumors in the spinal cord by MRI.

For MR imaging, we loaded the MRI contrast agent GdDTPA into the Fn-Rev-Ang nanocages to generate Fn-Rev-Ang-GdDTPA. Our T1 imaging experiments showed that Fn-Rev-Ang-GdDTPA rapidly (40 min) crossed the BBB. Next, we administered Fn-Rev-Ang-GdDTPA to glioma-bearing mice by tail vein injection to achieve brain delivery. Strikingly, gliomas with diameters below 1 mm and microscopic metastatic tumors in the spinal cord could be detected by MRI from the mice injected with Fn-Rev-Ang-GdDTPA. These MRI T1 results revealed that the tumor tissue gray signal intensity increased by 30%. We also observed pathological sections of tumor-bearing mouse brains by TEM and found that there is an intact BBB in the brains of tumor-bearing mice. Fn-Rev-Ang-GdDTPA provides a feasible method for diagnosing low-grade gliomas. Our results indicate that Fn-Rev-Ang would greatly extend the usage of Magnevist in microscopic tumors in the brain and spinal cord, which would overcome the limitations of the current clinical MRI technology.

In addition, Fn-Rev-Ang-loaded Dox (Fn-Rev-Ang-Dox) had an obvious inhibitory effect on mouse brain gliomas and their metastasis, which significantly prolonged the survival of the mice relative to mice treated with free Dox or controls. One possible reason for this result is that the receptors for angiopep-2 (LRP1) and ferritin (transferrin receptor) are both overexpressed in many cancer cells. Fn-Rev-Ang-Dox shows greater accumulation in cancer cells compared with that in normal cells.

CONCLUSIONS

We developed a novel dual-order targeted nanoparticle platform, Fn-Rev-Ang, as a strategy to diagnose and treat low-grade gliomas. Using Fn-Rev-Ang, the MRI contrast agent GdDTPA (Magnevist) can successfully identify the microscopic brain tumors (less than 1 mm) and metastatic spinal cord tumors in mice, which holds promise in extending the applications of Magnevist in the clinic. In addition, Fn-Rev-Ang-Dox not only prolonged the survival time of the mice, but also prevented metastasis of the brain tumor to the spinal cord. Above all, we propose that Fn-Rev-Ang can serve as a universal nanoplatform for the imaging and therapy of microscopic tumors in the brain and spinal cord.

MATERIALS AND METHODS

Design, Expression, Purification, and Characterization of Fn-Rev-Ang. Mutagenic HREV-107-Angiopep2-His proteins were conjugated to ferritin to generate Fn-Rev-Ang. The N-terminus of ferritin is exposed in the ferritin nanocage. *E. coli* was used to express proteins by constructing plasmids of target proteins The Rev-Ang-His protein was thus incorporated at the N-terminus of ferritin, and the resulting Fn-Rev-Ang protein was expressed in *E. coli*. Cultures (1 L each) of *E. Coli* (BL21) containing the pET-28a(+) Fn-Rev-Ang plasmid were grown for 8 h in ampicillin (100 mg/L). *E. Coli* was

https://dx.doi.org/10.1021/acsomega.0c03073
ACS Omega 2020, 5, 20653−20663

induced by isopropyl-β-d-1-thiogalactopyranoside (1.0 mM), which was incubated overnight at 16 °C. *E. Coli* were then collected by centrifugation (30 min, 12,000 rmp, 4 °C). After sonication on ice and centrifugation, the supernatant was purified by both column chromatography (Ni-NTA affinity chromatograph) and size exclusion chromatography. Fn-Rev-Ang was characterized by dynamic light scattering (DLS, Nano series-2S90), TEM (HITACHI-H-7650), SDS-polyacrylamide gel electrophoresis (PAGE), and ESI−MS. We chose a 0.22 μm filter. The protein was filtered to remove bacteria and stored at 4 °C. The protein concentration is about 2 mg/mL. The solution is a light yellow transparent liquid.

Dox and GdDTPA Encapsulation in the Fn-Rev-Ang Nanocage. Fn-Rev-Ang at a concentration of 2 mg/mL was dissolved in PBS (pH 7.4). The Fn-Rev-Ang solution was incubated for 5 min at pH 2.5 by adding hydrochloric acid (1.0 M). Dox hydrochloride or GdDTPA was then added to the solution at a 500:1 molar ratio of Dox hydrochloride or GdDTPA to Fn-Rev-Ang. The pH was then increased to 8.0 with NaOH (1.0 M). The solution was stirred at room temperature for 2 h, dialyzed with PBS at pH 7.4 to remove the free Dox or GdDTPA, and centrifuged at 12,000 rpm for 10 min at 4 °C. The supernatant was concentrated and stored at 4 °C. The Dox concentration was determined by measuring the absorbance at 485 nm, the GdDTPA concentration was determined by ICP−MS, and the concentration of Fn-Rev-Ang was determined by NanoDrop. The ratio of Dox:Fn-Rev-Ang was calculated to be 36:1, and the ratio of GdDTPA:Fn-Rev-Ang was 227:1 As shown in Figure S12, the protein particles are relatively stable after being loaded with small molecules. After high-speed centrifugation (using an ultrafiltration tube with a trapped volume of 3000 Da), the free small molecule filtrate on the right side is red, while the colorless filtrate on the left side is colorless. Through quantitative analysis, the loading amount of doxorubicin was found to be more than 90% in 60 h, and the filtrate almost did not contain DOX. Fn-Rev-Ang-GdDTPA data were determined using ICP−MS. The TEM image of Fn-Rev-Ang-Dox, Fn-Rev-Ang-GdDTPA, and Fn-Rev-Ang (pH = 6) are shown as Figure S13.

Confocal Fluorescence Microscopy Imaging. U87MG (ATCC) and HEK293T (ATCC) cells were cultured as recommended. Fluorescence microscopy images were collected using a Leica (Leica, Germany) confocal laser scanning microscope with a 63× oil immersion lens. Hoechst 33342 is useful for staining nuclei. It may be used for fluorescence microscopy. Hoechst 33342 was excited at 360 nm, and emission was detected at 480 nm. Cy5.5 was excited at 660 nm, and emission was detected at 710 nm. Dox was excited at 470 nm, and emission was detected at 590 nm. LysoTracker was excited at 440 nm, and emission was detected at 510 nm. U87MG and HEK293T cells were treated with 0.1, 0.2, or 0.4 μM Fn-Rev-Ang-Dox-Cy5.5 by incubation at 37 °C for 2 h. At the end of the incubation, the cells were washed and imaged.

***In Vitro* MRI Study.** A standard spin-echo sequence on a 3.0T MR scanner (Siemens AG, Germany) at room temperature was used to measure the relaxation time T1. Fn-Rev-Ang-GdDTPA solutions with different concentrations of Gd (0−1.0 mM) were prepared in PBS. After acquiring the T1-weighted MR images of x, the signal intensity of y was measured with selected ROI for each sample. The relaxation rates r_1 (1/T1) were measured from the relaxation time (T1) at various Gd concentrations. The T1-mapping image sequence is as follows: time of repetition (TR) = 500 ms, TE = 36.8 ms, field of vision (FOV) = 180 × 180 mm^2, slice = 5, slice thickness = 3 mm, and matrix size = 300 × 300.

***In Vivo* MRI Study.** U87MG cells (5 × 10^5, 10 μL) were injected into the right caudate (BALB/c nude mice with body weights of approximately 20 g) by using a stereotactic fixation device. A xenograft tumor with a diameter of 1.0 mm can be studied by MR imaging 10 days after inoculation. The mice with 20 g of body weight were anesthetized with chloral hydrate (7%) by intraperitoneal injection for the scans. T1 MRI (the TR was set to 500 ms, the TE was set to 11 ms, the flip angle was 150°, and the thickness was 0.8 mm; 3.0T SIEMENS) was used to observe the contrast enhancement generated every 2 min in the whole body after the tail vein injection of Fn-Rev-Ang-GdDTPA, Fn-GdDTPA, or GdDTPA (0.01 mM Gd/kg equivalents). To characterize the changes in signal intensity within the tumor tissues and other normal brain tissues for each agent over time, ROI analysis (select the imaging area and measure the gray scale) was performed on the T1 MR images using SIEMENS software (Multimodality Workplace).

Study on the Therapy of Tumor-Bearing Mice with Fn-Rev-Ang-Dox *in Vivo*. To evaluate the therapeutic effects of Fn-Rev-Ang-Dox in the U87MG tumor mouse model and compare these results with the same dose of the clinically approved free Dox, Fn-Rev-Ang-Dox (10 mg Dox/kg equivalents), PBS, and free Dox (2 mg/mL) were tail vein injected every 2 days into tumor-bearing mice after inoculation with U87MG cells into the right caudate for 10 days. Using the U87MG (expressing the luciferin gene)-bearing mouse model, we evaluated the glioma volume from the tumor bioluminescence intensity. The tumor bioluminescence intensities in the PBS-treated group increased rapidly, and spinal cord metastatic tumor signals were found in these animals. This suggested that the tumor was growing. The free Dox-treated group tumor signals remained unchanged. The Fn-Rev-Ang-Dox-treated group showed visible regression of tumor growth, which correlated well with the observed increase in survival in animals from this group.

■ ASSOCIATED CONTENT

Supporting Information

The Supporting Information is available free of charge at https://pubs.acs.org/doi/10.1021/acsomega.0c03073.

Materials and experimental procedures; additional TEM images; DLS, MRI, and fluorescence imaging efficiency of Fn-Rev-Ang2 NPs; cell imaging; H&E-stained images; and NP stability test (PDF)

■ AUTHOR INFORMATION

Corresponding Authors

Fugeng Sheng − *Chinese People's Liberation Army Hospital 307, Beijing 100071, China*; Email: fugeng_sheng@163.com

Jian Lin − *Synthetic and Functional Biomolecules Center, College of Chemistry and Molecular Engineering, Peking University, Beijing 100871, China*; orcid.org/0000-0002-1519-9679; Email: linjian@pku.edu.cn

Wu Zhong − *Beijing Institute of Pharmacology and Toxicology, Beijing 100850, China*; orcid.org/0000-0002-0536-620X; Email: zhongwu@bmi.ac.cn

https://dx.doi.org/10.1021/acsomega.0c03073
ACS Omega 2020, 5, 20653−20663

Authors

Zihao Wang − *Beijing Institute of Pharmacology and Toxicology, Beijing 100850, China*

Xinbo Zhou − *Beijing Institute of Pharmacology and Toxicology, Beijing 100850, China*

Yuru Xu − *Beijing Institute of Pharmacology and Toxicology, Beijing 100850, China*

Shiyong Fan − *Beijing Institute of Pharmacology and Toxicology, Beijing 100850, China*

Ning Tian − *Chinese People's Liberation Army Hospital 307, Beijing 100071, China*

Wenyuan Zhang − *Synthetic and Functional Biomolecules Center, College of Chemistry and Molecular Engineering, Peking University, Beijing 100871, China*

Complete contact information is available at: https://pubs.acs.org/10.1021/acsomega.0c03073

Author Contributions

Conceived and designed the experiments: W.Z., J.L. Imaging research and analysis: F.S., N.T. Performed the experiments (first author): Z.W. Contributed reagents/materials/analysis tools: X.Z., W.Z., S.F., Y.X.

Notes

The authors declare no competing financial interest.

All animals were kept in a pathogen-free environment. The procedures for care and use of animals were approved by the Ethics Committee of the Beijing Institute of Pharmacology and Toxicology, and all applicable institutional and governmental regulations concerning the ethical use of animals were followed.

■ ACKNOWLEDGMENTS

We are grateful for the financial support of the National Science and Technology Major Projects, under the program "Major New Drugs Innovation and Development" (2018ZX09711003) of China.

■ REFERENCES

(1) Dunn, G. P.; Rinne, M. L.; Wykosky, J.; et al. Emerging insights into the molecular and cellular basis of glioblastoma. *Genes Dev.* **2012**, *26*, 756−784.

(2) Cloughesy, T. F.; Cavenee, W. K.; Mischel, P. S. Glioblastoma: from molecular pathology to targeted treatment. *Annu. Rev. Phytopathol.* **2014**, *9*, 1−25.

(3) Flanigan, P. M.; Jahangiri, A.; Kuang, R.; et al. Developing an Algorithm for Optimizing Care of Elderly Patients With Glioblastoma. *Neurosurgery* **2018**, *82*, 64−75.

(4) Dhermain, F. G.; Hau, P.; Lanfermann, H.; Jacobs, A. H.; van den Bent, M. J. Advanced MRI and PET imaging for assessment of treatment response in patients with gliomas. *Lancet Neurol.* **2010**, *9*, 906−920.

(5) Ewelt, C.; Floeth, F. W.; Felsberg, J.; et al. Finding the anaplastic focus in diffuse gliomas: the value of Gd-DTPA enhanced MRI, FET-PET, and intraoperative, ALA-derived tissue fluorescence. *Clin. Neurol. Neurosurg.*. **2011**, *113*, 541−547.

(6) Yan, H.; Wang, L.; Wang, J.; et al. Two-order targeted brain tumor imaging by using an optical/paramagnetic nanoprobe across the blood brain barrier. *ACS Nano* **2012**, *6*, 410−420.

(7) Demeule, M.; Currie, J. C.; Bertrand, Y.; et al. Involvement of the low-density lipoprotein receptor-related protein in the transcytosis of the brain delivery vector angiopep-2. *J. Neurochem.* **2008**, *106*, 1534−1544.

(8) Nam, H. Y.; Nam, K.; Hahn, H. J.; et al. Biodegradable PAMAM ester for enhanced transfection efficiency with low cytotoxicity. *Biomaterials* **2009**, *30*, 665−673.

(9) Davis, M. E.; Chen, Z.; Shin, D. M. Nanoparticle therapeutics: an emerging treatment modality for cancer. *Nat. Rev. Drug Discovery* **2008**, *7*, 771−782.

(10) Wang, J.; Sui, M.; Fan, W. Nanoparticles for tumor targeted therapies and their pharmacokinetics. *Curr. Drug Metab.* **2010**, *11*, 129−141.

(11) Harrison, P. M.; Arosio, P. The ferritins: molecular properties, iron storage function and cellular regulation. *Biochim. Biophys. Acta, Bioenerg* **1996**, *1275*, 161−203.

(12) Khoshnejad, M.; Parhiz, H.; Shuvaev, V. V.; Dmochowski, I. J.; Muzykantov, V. R. Ferritin-based drug delivery systems: Hybrid nanocarriers for vascular immunotargeting. *J. Controlled Release* **2018**, *282*, 13−24.

(13) Huang, X.; Chisholm, J.; Zhuang, J.; Xiao, Y.; Duncan, G.; Chen, X.; et al. Protein nanocages that penetrate airway mucus and tumor tissue. *Proc. Natl. Acad. Sci. U.S.A.* **2017**, *114*, E6595−E6602.

(14) Chen, L.; Bai, G.; Yang, R.; Zang, J.; Zhou, T.; Zhao, G. Encapsulation of beta-carotene within ferritin nanocages greatly increases its water-solubility and thermal stability. *Food Chem.* **2014**, *149*, 307−312.

(15) Du, B.; Jia, S.; Wang, Q.; et al. A Self-Targeting, Dual ROS/pH-Responsive Apoferritin Nanocage for Spatiotemporally Controlled Drug Delivery to Breast Cancer. *Biomacromolecules* **2018**, *19*, 1026−1036.

(16) Fan, K.; Gao, L.; Yan, X. Human ferritin for tumor detection and therapy. *Wiley Interdiscip. Rev.: Nanomed. Nanobiotechnol.* **2013**, *5*, 287−298.

(17) Zhang, Y.; Orner, B. P. Self-assembly in the ferritin nano-cage protein superfamily. *Int. J. Mol. Sci.* **2011**, *12*, 5406−5421.

(18) Geninatti Crich, S.; Bussolati, B.; Tei, L.; et al. Magnetic resonance visualization of tumor angiogenesis by targeting neural cell adhesion molecules with the highly sensitive gadolinium-loaded apoferritin probe. *Cancer Res.* **2006**, *66*, 9196−9201.

(19) Yang, Z.; Wang, X.; Diao, H.; et al. Encapsulation of platinum anticancer drugs by apoferritin. *Chem. Commun.* **2007**, 3453−3455.

(20) Lin, X.; Xie, J.; Niu, G.; et al. Chimeric ferritin nanocages for multiple function loading and multimodal imaging. *Nano Lett.* **2011**, *11*, 814−819.

(21) Li, L.; Fang, C. J.; Ryan, J. C.; Niemi, E. C.; Lebrón, J. A.; Björkman, P. J.; et al. Binding and uptake of H-ferritin are mediated by human transferrin receptor-1. *Proc. Natl. Acad. Sci. U.S.A.* **2010**, *107*, 3505−3510.

(22) Cao, C.; Wang, X.; Cai, Y.; et al. Targeted in vivo imaging of microscopic tumors with ferritin-based nanoprobes across biological barriers. *Adv. Mater.* **2014**, *26*, 2566−2571.

(23) Lillis, A. P.; Van Duyn, L. B.; Murphy-Ullrich, J. E.; Strickland, D. K. LDL receptor-related protein 1: unique tissue-specific functions revealed by selective gene knockout studies. *Physiol. Rev.* **2008**, *88*, 887−918.

(24) Johnsen, K. B.; Burkhart, A.; Melander, F.; et al. Targeting transferrin receptors at the blood-brain barrier improves the uptake of immunoliposomes and subsequent cargo transport into the brain parenchyma. *Sci. Rep.* **2017**, *7*, 10396.

(25) Candela, P.; Saint-Pol, J.; Kuntz, M.; Boucau, M.-C.; et al. In vitro discrimination of the role of LRP1 at the BBB cellular level: focus on brain capillary endothelial cells and brain pericytes. *Brain Res.* **2015**, *1594*, 15−26.

(26) Guo, J.; Xu, N.; Yao, Y.; Lin, J.; Li, R.; Li, J.-W. Efficient expression of recombinant human heavy chain ferritin (FTH1) with modified peptides. *Protein Expression Purif.* **2017**, *131*, 101−108.

(27) Uchida, M.; Flenniken, M. L.; Allen, M.; et al. Targeting of cancer cells with ferrimagnetic ferritin cage nanoparticles. *J. Am. Chem. Soc.* **2006**, *128*, 16626−16633.

(28) Ren, X.; Lin, J.; Jin, C.; Xia, B. Solution structure of the N-terminal catalytic domain of human H-REV107–a novel circular permutated NlpC/P60 domain. *FEBS Lett.* **2010**, *584*, 4222−4226.

(29) Vecchione, D.; Aiello, M.; Cavaliere, C.; Nicolai, E.; Netti, P. A.; Torino, E. Hybrid core shell nanoparticles entrapping Gd-DTPA

and (18)F-FDG for simultaneous PET/MRI acquisitions. *Nanomedicine* **2017**, *12*, 2223−2231.
(30) Vré, R. M.-D.; Lemort, M. Invited review: biophysical properties and clinical applications of magnetic resonance imaging contrast agents. *Br. J. Radiol.* **1995**, *68*, 225−247.
(31) Bui, T.; Stevenson, J.; Hoekman, J.; Zhang, S.; Maravilla, K.; Ho, R. J. Y. Novel Gd nanoparticles enhance vascular contrast for high-resolution magnetic resonance imaging. *PLoS One* **2010**, *5*, No. e13082.
(32) El-Zawahry, A.; McKillop, J.; Voelkel-Johnson, C. Doxorubicin increases the effectiveness of Apo2L/TRAIL for tumor growth inhibition of prostate cancer xenografts. *BMC Cancer* **2005**, *5*, 2.

https://dx.doi.org/10.1021/acsomega.0c03073
ACS Omega 2020, 5, 20653−20663